Exp Fluids (2013) 54:1437
DOI 10.1007/s00348-012-1437-7

RESEARCH ARTICLE

# Plunging to spilling transition in corner surface waves in the wake of a partially submerged vertical plate

**P. Martínez-Legazpi · J. Rodríguez-Rodríguez · C. Marugán-Cruz · J. C. Lasheras**

Received: 25 May 2012 / Revised: 7 September 2012 / Accepted: 10 December 2012


**Abstract** We describe the downstream flow developing at the corner of a partially immersed flat plate, placed perpendicular to a uniform stream. As the flow converges toward the plate centerline, a steady wave, which remains attached to the corner of the plate, develops downstream. Both the amplitude and slope of the wave increase with the downstream distance until the wave either gently spills or plunges depending on the flow conditions. We show that this "corner wave" can be used as a prototypical flow to study the breaking process of two-dimensional deep-water surface waves allowing for the application of a variety of measurement techniques to characterize their evolution. We propose a criterion, based on the Froude number, to determine the transition from spilling to plunging for two-dimensional surface gravity waves consistent with a large set of experimental observations obtained in this flow configuration.

## 1 Introduction

The breaking of surface gravity waves in deep water plays a very important role in the air–sea interaction and in the energy exchange in the oceans, and it is strongly related to some issues of paramount importance both in the field of oceanography as well as in naval hydrodynamics. The behavior of surface gravity waves is essential to the quantification of the drag force experienced by ships (Newman 1977), the mass and energy transfer between the ocean and the atmosphere (Melville 1996), the development of accurate tools for ship-maneuvering modeling (Molland 2008), and the design of reliable marine structures (Sumer and Fredsoe 1997), among many other technological and natural phenomenona.

According to its breaking behavior, surface waves have been classified as follows: "plunging breakers," in which the crest separates from the wave and plunges into the free surface (Galvin Jr 1968), and "spilling waves," in which the crest tumbles down the front (or face) of the wave, (Duncan et al. 1994). There are extensive and comprehensive reviews of the physics that lead to one or another wave behavior (Cokelet 1977; Duncan 2001; Banner and Peregrine 1993; Kiger and Duncan 2011), and a variety of criteria have been proposed to determine when the crest of a wave will either spill or plunge (see f.e. Rapp and Melville 1990; Schultz et al. 1994; Oh et al. 2005 or Bonmarin and Ramamonjiarisoa 1985). However, due in part to the highly non-stationary nature of the breakage, there is no unified criterion for this transition. Many of the discrepancies in these criteria are due to the difficulty in directly measuring the wave flow field and the surface slope in an unsteady reference frame.

Over the years, wave breaking has been studied in the laboratory in a variety of ways. One of the most commonly used devices to generate waves in open water tanks are mechanical wave-makers. A paddle or a piston (or even a fan) generates a momentum source to the adjacent fluid, producing a surface wave that advances along the channel until, due to nonlinear effects or changes in the geometry of the channel, it breaks (see, that is, Melville and Rapp 1988

P. Martínez-Legazpi (✉) · J. Rodríguez-Rodríguez · C. Marugán-Cruz
Fluid Mechanics Group, Universidad Carlos III de Madrid, Av. Universidad 30., 28911 Leganés, Spain
e-mail: pmartine@ing.uc3m.es

J. C. Lasheras
Department of Mechanical and Aerospace Engineering, University of California San Diego, 9500 Gilman Dr. La Jolla, San Diego, CA 92093, USA

Published online: 23 December 2012

and references therein). Among others, the advantages of wave-makers include the ability to create trains of waves of variable frequency and amplitude, thereby ensuring the emergence of both plunging and spilling breakers. However, despite being the method most often used to study this phenomenon in the laboratory, the waves are not stationary, making the measurement difficult and in some cases resulting in a lack of resolution and repeatability.

An alternative way to generate stationary waves in a laboratory frame is by using a submerged hydrofoil in a re-circulating water channel (Duncan 1981). This technique grants the formation of a stationary wave in the laboratory reference frame, thus allowing the implementation of accurate experimental techniques. The resistance of the body manifests itself as a perturbation on the free surface which grows as a wave. The submerged hydrofoil has been widely used to study spilling waves or bores, but obviously, it can not produce steady plunging breakers, as they can not exist in a two-dimensional flow.

Breakers in a water tank can also be produced by transmitting the necessary momentum to the fluid through a hydrostatic pressure source, instead of directly accelerating the stream near the free surface, as in the case of the submerged hydrofoil, or using the mechanical paddle of a wave-maker. The basis of this method consists of inducing a horizontal velocity, $\sqrt{g\Delta h}$, to a certain amount of fluid at rest by suddenly releasing an adjacent water mass of height $\Delta h$ as outlined in Fig. 1. Although the generation of internal and surface gravity waves has been extensively studied using this method (Mauer et al. 2010), it presents significant experimental complications in the generation of plunging surface waves. These complications are mainly due to the necessity of setting up a system of lock-gates in order to initially isolate both zones and the perturbation effect caused by the sudden withdraw of the gate.

The "corner wave" flow we studied represents an alternative experimental way to generate, in a recirculating water channel, the idealized flow condition shown in Fig. 1 without the complications introduced by the gates or other mechanisms. Furthermore, the waves we studied are stationary in the laboratory reference frame, allowing the implementation of very accurate measurement techniques. In our experiments, we have taken advantage of the slender nature of the supercritical flows through the use of the so called 2D+T approximation.

Such approximation takes advantage of the duality between two-dimensional unsteady flows and steady, slender three-dimensional flows, and it is commonly known as 2D+1/2 or 2D+T approximation. The 2D+T approximation was first proposed by Munk (1924) to study the aerodynamics of slender bodies. Wagner (1932), made use of it to formally associate the problem of a slender body planing on water with that of a plate impacting on a free surface. Tulin adapted this method for the analysis of high-speed surface ships, (Tulin 1957), and showed that this method can be used with very good results for ships at sufficiently high speed ("supercritical flow") (Tulin and Wu 1997). Since then, the applications of the 2D+T approximation in naval hydrodynamics have been numerous and fruitful (see the review article by Fontaine and Tulin 1998 and references therein). More recently, the 2D+T approximation has also been used to study experimentally the dynamics of bow waves produced by slender hulls in a laboratory water channel (Shakeri et al. 2009a, b). In these studies, it was found that the 2D+T approximation was in excellent agreement with fully 3D RANS calculations (Iafrati and Broglia 2010).

Before finishing this introduction, and as a historical note, it would be worth mentioning that the flow studied in this paper was sketched originally in the sixteenth century by Leonardo da Vinci (Richter 1970). One of da Vinci's drawings is reproduced here in Fig. 2.

## 2 Experimental methodology

For the sake of clarity, let us provide first a brief statement of the problem. Consider the supercritical flow around a partially submerged vertical plate placed perpendicular to a uniform stream in a re-circulating water channel. Let the channel width $W'$ be much larger than the plate width $W_0$ as shown in Fig. 3a. In the formulation of the problem, the streamwise, spanwise, and vertical coordinates are denoted as $x'$, $y'$, and $z'$, respectively, and the origin of coordinates is placed at the submerged corner of the plate. The lower edge of the plate is at a distance $h_g$ above the bottom of the

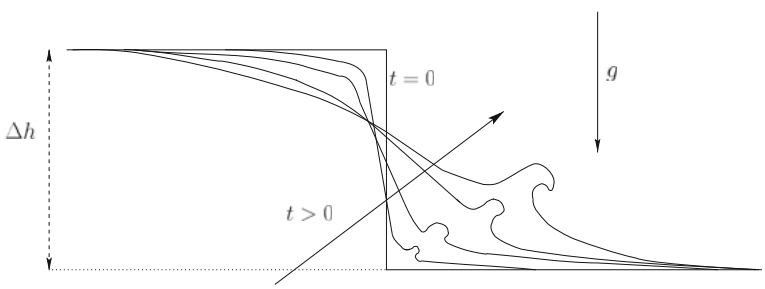


**Fig. 1** Sketch of the unsteady free surface evolution after using an hydrostatic pressure source to generate breaking waves in the laboratory frame

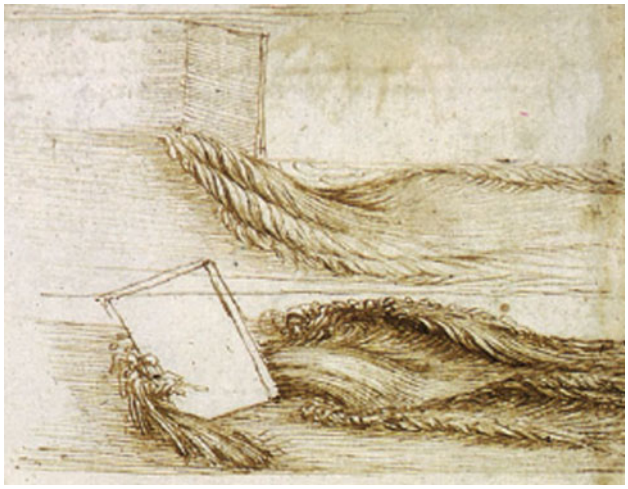

**Fig. 2** Leonardo da Vinci, Study of water passing obstacles, c. 1508-9

channel, whereas the water level upstream from the plate has a depth $h_0$ as shown in Fig. 3b.

Except for a region near the corner where three-dimensional effects are important, the flow downstream from the plate behaves exactly as a two-dimensional sluice gate: after a short distance where the depth decreases due to the *vena contracta* effect, a uniform height $h_1 < h_g$ is attained. Under these conditions, the velocity distribution in the region of depth $h_1$ has a uniform value, $U_1$, as has been reported in similar flows (Kim 2007; Roth and Hager 1999).

The depth, $h_g$, the reference water level in the ideal two-dimesional problem, is used as a reference to define the characteristic length scales; $\delta = (h_g - h_1)$ and $\Delta h = (h_0 - h_g)$. The former is the reduction of the depth due to the *vena contracta*, whereas the latter is the maximum height difference of the free surface found in the ideal two-dimensional case and is used to define the Froude number,

$$Fr_{\Delta h} = \frac{U_1}{\sqrt{g\Delta h}}. \quad (1)$$

When the Froude number is large enough, $Fr > 1$, a three-dimensional steady wave, anchored at the plate's corner, forms. This "corner wave" is stationary in the laboratory reference frame. Similar to deep-water waves, the crest of this wave advances along the spanwise direction while the wave amplitude grows, which eventually leads, depending on the flow parameters, to the formation of either a plunging or a spilling breaker. As will be shown later, a remarkable characteristic of the corner wave is that its evolution and breaking characteristics are relatively unaffected by the presence of the channel's side and bottom walls, even when their distance to the wave is comparable to the wave amplitude.

Hager and Yasuda (1997) and Hager and Mazumder (1992) have studied the flow in a sudden expansion of a channel. Although the sudden expansion problem has some similarities to our flow, the fact that the wave formed there propagates on a dry basin makes the problem analogous to the classical dam-break problem when treated with the 2D+T approximation. Nonetheless, the existence of a wet basin in our case makes it rather different from these problems.

The experiments were carried out in a re-circulating water channel. The channel had a capacity of about five cubic meters. The test section was 2 m long with a [0.6 m × 0.6 m] square cross–section, as sketched in Fig. 4. The plenum was connected to the test section by a series of grids and honeycombs, followed by a contraction, to ensure that the fluctuations originating at the pump were damped out before the flow reached the test section. Three polished plexiglas plates of different widths [0.3, 0.5, and

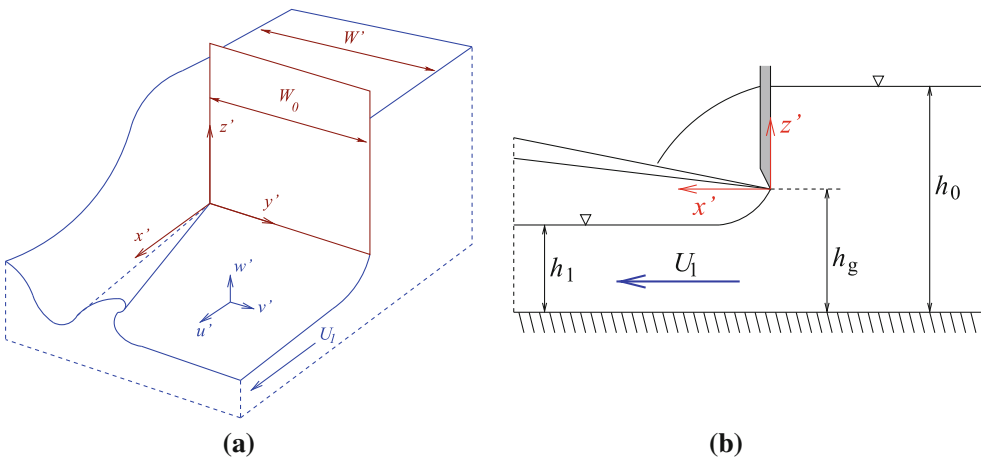


**Fig. 3** Sketch of the flow setup. **a** General view. **b** Side ($x'$–$z'$) view

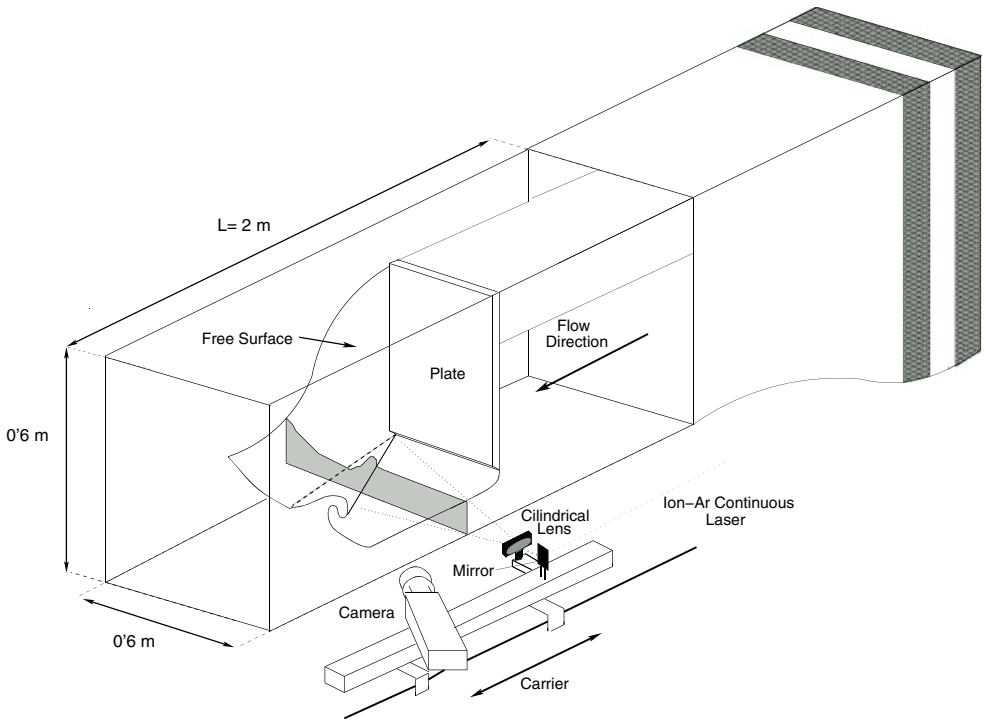


**Fig. 4** Sketch of the re-circulating channel and the laser induced fluorescence (LIF) setup. The laser sheet, parallel to the plate, passes through the free surface of the flow which is captured by a CCD camera attached to the traverse

0.7 times the channel width (0.6 m)], and thickness 0.0127 m, were manufactured, placed vertically across the test section, and fixed to one of the walls of the water channel to produce the corner wave. The ends of the plates that induced the flow were machined to a sharp edge so that the free stream detaches cleanly from the gate without any possible boundary layer growth that would perturb the experiment and hinder its reproducibility. Finally, the underlying turbulent intensity of the free stream measured from previous experiments (Aliseda and Lasheras 2006; Rodríguez-Rodríguez et al. 2011) was very low, less than 0.5 %.

In all cases, several velocity profiles were measured in the region of constant height $h_1$. In each case, the velocity profile upstream from the plate was measured using a PIV technique to ensure its uniformity (Roth and Hager 1999). A detailed explanation of such measurements can be found in Martínez-Legazpi (2011). Pitot tubes were also used to monitor $U_1$ through all the experiments.

### 2.1 Laser induced fluorescence (LIF)

A series of laser induced fluorescence (LIF) measurements were performed in the channel. To that end, a 7W Ion-Argon laser beam (Coherent Innova 90) operating in all lines mode was mounted on an optical table near the channel, as shown in Fig. 4. The beam was aligned parallel to the lateral walls of the test section using a set of mirrors. One additional mirror, mounted in a traverse parallel to the wall, was used to direct the beam perpendicular to the test section, lined up with the plate. A combination of cylindrical and spherical lenses were used to produce a laser sheet in the plate's plane ($y'$–$z'$). In addition, the water ($\sim 5$ $m^3$) was seeded with around 50 g of fluorescein ($\sim 10$ ppm) in order to facilitate the visualization of the flow.

The intersection of the flow with the laser sheet was captured using a digital (CCD) camera (Kodak Megaplus 1.0 ES) with a resolution of 1008 × 1010 pixels, together with a NIKON lens of 30 mm of focal distance and 1.4f. A band-pass filter was placed in front of the lens to avoid any direct reflections from the laser. The viewing direction of the camera was set at an angle of 45° to the normal of the laser sheet to ensure optimal spatial resolution. Calibration images were acquired using a grid attached to the downstream face of the plate, as shown in Fig. 7d. The laser sheet and the camera, placed on the same traverse, were moved together in the streamwise direction, thus ensuring that the camera was always focused on the light sheet.

The field of view of the camera was about 0.4 m, corresponding to a resolution of approximately 2.5 px/mm. In the proximity of the plate, where the wave is starting to develop and the free surface shape is smooth, its location could be determined with an accuracy of ±3 mm, taking into account all possible experimental errors. However, in regions where the free surface shape was more complex as the region near the splash of plunging breakers, the accuracy of the method was estimated to be ±6 mm.

Once the images were acquired, the location of the free surface was determined by an image processing routine written in MATLAB (R2011a, 2011). Figure 5 shows the

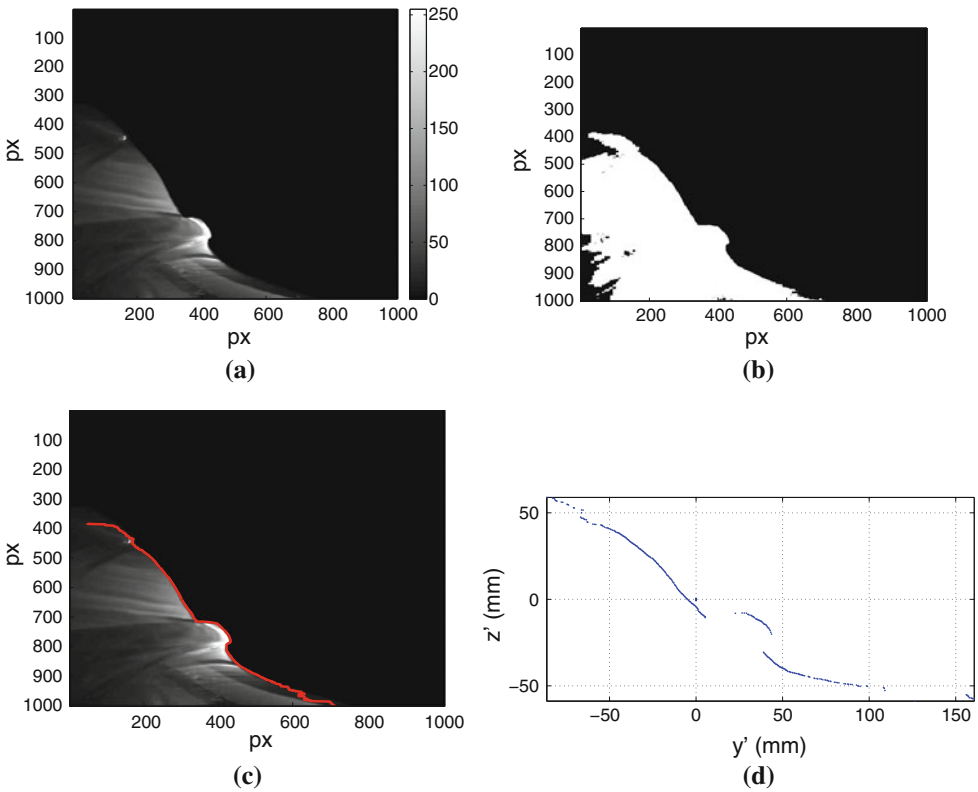


**Fig. 5** Image processing routine used in the LIF experiments. **a** Raw cross-view image of a plunging breaker in which the lateral bar represents the gray intensity in each pixel. **b** Results of applying a binary threshold to **a**. **c** Free surface location after using an edge detection algorithm. **d** Free surface location in the original axis. Notice that by illuminating the flow from the side of the channel, the parts of the free surface with negative or horizontal slopes cannot be precisely determined and should be removed from the results

different steps of such process. In Fig. 5a, a raw acquired image is shown together with the gray intensity levels of each pixel. Notice that when illuminating the flow, the addition of fluorescein allows the visualization only of the section bisected by the laser beam and its downstream development. Hence, as shown in Fig. 5b, a threshold can be applied to the image to convert the regions with less gray intensities to a single one with an assigned value of gray intensity. The process can be similarly applied to the other areas of the image. Therefore, the gray intensity gradient can be used as a marker to determine the position of the free surface, as shown in Fig. 5c. It is important to notice that by illuminating from one side of the channel, there are regions of the free surface which, depending on its curvature, can create shadows in the image. The existence of shadows in the image leads to errors in the determination of the interface. In this study, all the regions of the free surface in which negative or zero vertical slopes were observed were declared invalid and removed from the final result to minimize this effect.

### 2.2 Determination of the wave trajectories in the $x$–$y$ plane

High-resolution image processing was conducted in a large set of experimental conditions. The images were taken using the same camera as the one used in the LIF experiments described previously. The images were acquired in two specific locations: from above, with the aim of detecting the trajectory of the leading and trailing edges of the wave, and, from the side, with the objective of obtaining the characteristic heights in each of the flow conditions.

An example of one of these images is shown in Fig. 6a, whereas Fig. 6b illustrates the detection of both edges using an image processing routine written in MATLAB. By definition, the leading edge corresponds to the line in which the maximum steepness (vertical) of the free surface is attained, whereas the trailing edge is located at the depression, or valley, which is left behind the wave in its development. This valley marks the inception of the divergent wave which also forms in these types of flows. The error in the identification of the location of the front was estimated to be of the order of the height of the capillary ripples $\sim\pm5$ mm. However, for the valley, the error increases up to $\pm10$ mm, due to the absence of a steep free surface shape in that location. Steep free surface shape usually produces large light reflections and therefore, large light intensity gradients in the acquired image, facilitating the post- processing.

## 3 Results and discussion

We performed a parametric study to investigate the dependence of the breaker configuration on the flow speed,

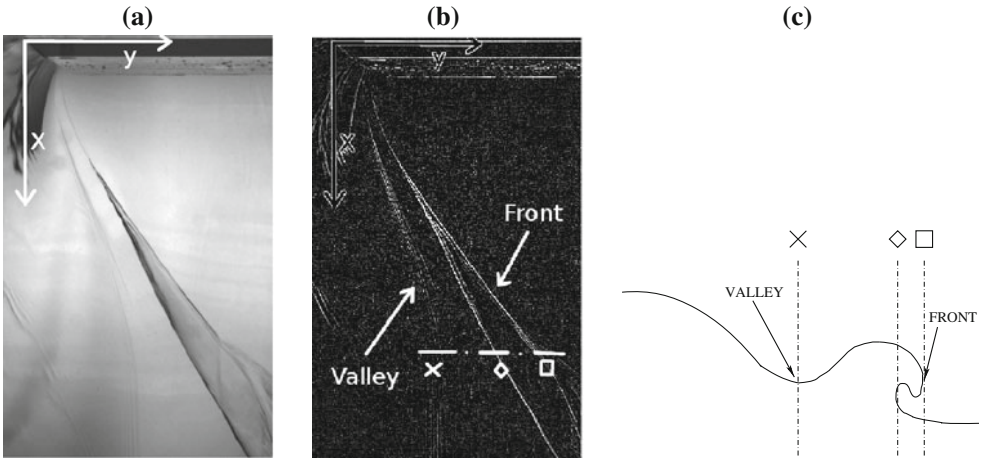


**Fig. 6** Image processing method. **a** *Top* view of a typical plunging breaker. Notice that the *shaded* region of the wave coincides with the overturning of the crest. **b** Edge detection algorithm with the front (leading edge) and valley (trailing edge) identification. **c** Sketch of the cross-section view identified in **b** as the *dash-dotted line*

**Table 1** Summary of some representative experimental conditions, where $W = W_0/W'$ is the non-dimensional width of the plate, $h_0$ the water level upstream the plate, $h_1$ the water level downstream the plate, and $h_g$ the height of the lower edge of the plate with respect to the basin. The experimental error in the determination of all the heights involved in this work was estimated to be ±2 mm

| | $W$ | $h_g$ (mm) | $h_1$ (mm) | $h_0$ (mm) | $\Delta h$ (mm) | $\delta$ (mm) | $U_1$ (m/s) | $Fr_{h_g}$ | $Fr_{\Delta h}$ | $Fr_g$ |
|---|---|---|---|---|---|---|---|---|---|---|
| A | 0.5 | 155 | 105 | 310 | 155 | 50 | 2.09 | 1.69 | 1.69 | 3.01 |
| B | 0.5 | 155 | 105 | 252 | 97 | 50 | 1.84 | 1.49 | 1.88 | 2.62 |
| 1 | 0.5 | 95 | 58 | 374 | 279 | 37 | 2.48 | 2.57 | 1.50 | 4.11 |
| 2 | 0.5 | 95 | 58 | 352 | 257 | 37 | 2.41 | 2.49 | 1.52 | 4.01 |
| 3 | 0.5 | 95 | 58 | 239 | 144 | 37 | 1.94 | 2.01 | 1.63 | 3.22 |
| 4 | 0.5 | 162 | 108 | 306 | 144 | 54 | 1.95 | 1.55 | 1.64 | 2.68 |
| 5 | 0.7 | 140 | 93 | 257 | 117 | 47 | 1.71 | 1.46 | 1.60 | 2.52 |
| 6 | 0.3 | 118 | 77 | 230 | 112 | 41 | 1.75 | 1.63 | 1.67 | 2.76 |

$U_1$, and the characteristic length scales, $\Delta h = (h_0 - h_g)$ and $\delta = (h_g - h_1)$. Table 1 summarizes some of the experimental conditions used, as well as the value of the Froude numbers based on $h_g$, defined as $Fr_{h_g} = U_1/\sqrt{gh_g}, \Delta h$, previously defined as $Fr_{\Delta h} = U_1/\sqrt{g\Delta h}$, and $\delta$, defined as $Fr_g = U_1/\sqrt{g\delta}$.

### 3.1 Free surface evolution

The LIF technique was applied to track the evolution of the free surface in the two typical breaker configurations, plunging and spilling, identified in Table 1 as cases A and B. Figure 7a shows the free surface evolution of the case A. This case corresponds to a typical plunging breaker. Notice that the curl of the crest produces shadow regions that limit the ability of the technique to characterize the totality of the free surface location in this configuration. To illustrate this effect, a red line representing the shape of a plunging breaker is added to the figure. Figure 7b, shows the free surface evolution of the case B of Table 1. In this figure, it can be noted that the wave becomes steeper as it evolves until the crest becomes unstable, resulting in white water spilling down the face of the wave, as described by Duncan (Duncan et al. 1999). Figure 7c, shows the time evolution of the initial free surface, of case A in Table 1, calculated using a boundary element method under the 2D+T approximation (for numerical details see Martínez-Legazpi 2011). To facilitate the comparison with (c), in (a) and (b), all magnitudes are made dimensionless with the width of the channel (Martínez-Legazpi 2011).

It must be pointed out that the 2D+T approximation is readily applicable to our flow. In a general case, the 2D+T approximation can be applied when a liquid is moving with a uniform speed, $U$ ($U_1$ in our flow) and is steadily perturbed by height differences of size, $h$ (corresponding to the characteristic wave heights in this study), having $U \gg (gh)^{1/2}$. Under these conditions, a perturbation would propagate laterally (i.e., perpendicularly to the free stream) with speeds of the order $v \sim (gh) \ll U$. Therefore, by the time the perturbation has moved laterally a distance, $y$, it has been advected by the free stream, a distance $L \sim yFr_h \gg y$, where $Fr_h = U/(gh)^{1/2}$ is the Froude number. In all our experiments, the flow can be considered locally slender, with

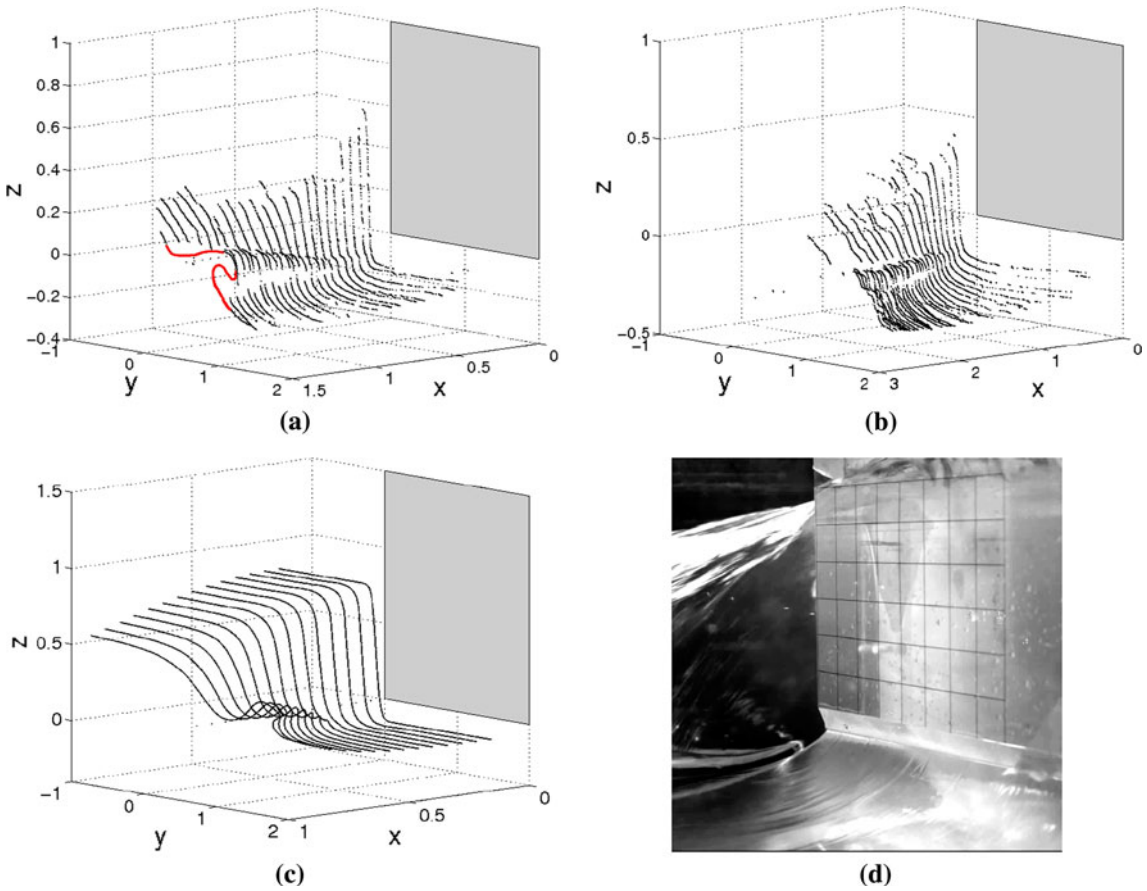


**Fig. 7** LIF Results of the different breaking conditions: **a** plunging breaker. **b** Spilling breaker. The plunging breaker corresponds to case A in Table 1 and the spilling one to case B. A *dotted line* marking the *corner* of the plate is plotted together as a reference in both figures. To clarify the plunging configuration, a sketch of the real free surface, plotted in *red*, is added in **a**, showing the limitations of the method. **c** Numerical result of the plunging breaker (**a**), using a 2D+T approximation code, as described in Martínez-Legazpi (2011). **d** LIF calibration grid

an aspect ratio of the order of the inverse of the Froude number. More importantly, since variations in the streamwise velocity component are also of order $v$, the advection of the perturbation wave nearly occurs at the uniform velocity, $U$, which further justifies the validity of the 2D+T formulation of slender flows. Therefore, one can conclude that in all our experiments, regardless of the moderate values of the Froude number, $Fr_{\Delta h}$, the 2D+T approximation can be applied to our "corner wave." This is justified when considering that the local Froude number, based on wave height, $h$, $Fr_h \sim O(10)$, fulfills the slenderness criterion necessary for the implementation of such transformation.

### 3.2 Wave trajectories and influence of the channel walls

The dimensional parameter that controls the depth of penetration of the plate is the height of its lower edge, $h_g$. In dimensionless terms, this parameter yields a Froude number, $Fr_{h_g} = U_1/\sqrt{gh_g}$. The influence of this parameter on the wave trajectories, compared to the previously defined Froude number, based in the maximum difference of heights of the free surface, $Fr_{\Delta h} = U_1/\sqrt{g\Delta h}$, can be seen in Fig. 8a, where the trajectories of three different waves, identified as cases 1–3 in Table 1, are plotted. The first three trajectories were obtained keeping the Froude number $Fr_{\Delta h}$ constant, while varying $Fr_{h_g}$. Figure 8a reveals that moderate variations ($\sim$20 %) of the Froude number based on the distance $h_g$ do not produce significant changes in the trajectory of the wave. This result reveals that the corner wave is not affected by the presence of the bottom in the range of parameters that we have used in all our experiments reported here. Indeed, the fact that the trajectories of cases 1–3 are nearly identical, where $U_1$ changes while $h_1$ is kept constant, indicates that the spanwise velocity of the wave is proportional to $U_1$ rather than to $\sqrt{gh_1}$ as would be the case in a shallow water wave.

Considering the possible influence of the lateral channel walls, we conducted similar experiments, cases 4–6 in Table 1, keeping $Fr_{\Delta h}$ constant, while changing the plate's

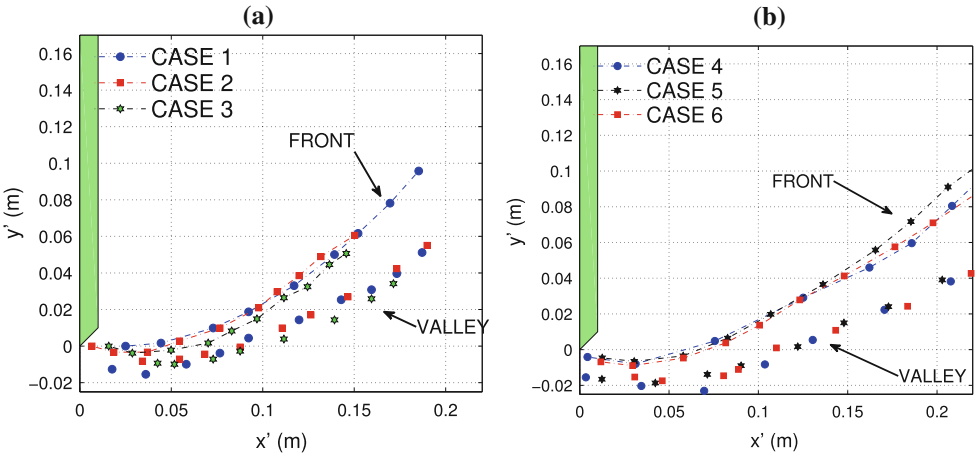


**Fig. 8** Wave front and valley trajectories. **a** Wave trajectories of cases 1–3 of Table 1. **b** Wave trajectories of cases 4–6 of Table 1, obtained using three different plates of $W = 0.3$, 0.5 and 0.7 for the same $Fr_{\Delta h}$. In both figures, *the dash-dotted line* represents the leading edge trajectory

width. Figure 8b shows the wave trajectories in a region close to the plate for three experiments performed with different plate's widths ($W = 0.3$, 0.5 and 0.7) and similar $Fr_{\Delta h}$ It can be seen that the influence of the width of the plate on the wave trajectory is negligible.

With the above results in mind, we can conclude that, for all the experiments reported here, the wave trajectories depend only on the Froude number, $Fr_{\Delta h}$. However, it is important to point out that our analysis is expected to remain valid only as long as the corner wave trajectories do not interact with the boundary layers at the channel walls. The results shown in Fig. 8 confirm that the corner wave formation is a local phenomenon which is mainly driven by the conditions near the corner of the plate and is not affected by the solid boundaries of the channel.

### 3.3 Ballistic trajectories of the wave front

It is well known that in deep-water plunging breakers, the sheet ejected after the separation of the crest, hereafter referred to as the jet, follows a ballistic trajectory in its evolution. Previous works, and in particular that of Longuet-Higgins, describe theoretically that "when the tangent of the free surface of the wave near the crest makes a sharp right-angle turn, there is a large pressure gradient in the fluid that accelerates the fluid near the crest horizontally and propels a jet forward from the crest. In this state, the jet narrows rapidly, and the pressure gradient within the jet diminishes drastically; the fluid is then almost in a state of a free fall in a parabolic trajectory" (Longuet-Higgins 1995). This assertion has been verified experimentally, among others, by Shakeri et al. (2009) or Drazen et al. (2008).

Assuming, for the sake of the argument, that the crest of the corner wave behaves similarly to that of a deep-water wave, it would, therefore, be natural to define the range of its ballistic path, $x_r$, as the distance between the separation point, that occurs in the vicinity of the corner of the plate, and the point where the jet impacts on the free surface downstream from the plate in the downstream direction. This assumption is motivated by the observation of Figs. 6a and 9a, where the front of the corner wave is seen to follow a straight line starting almost at the plate. It should be emphasized that, contrary to the wave trajectory, the range of the ballistic trajectory in the $(y'–z')$ plane is shown to be more sensitive to $\delta$ than to $\Delta h$.

Following the ballistic flight theory, the range $x_r$ should scale with the time of flight of a particle falling a distance equal to the height of the plate edge with respect to the free surface, $\delta = (h_g - h_1)$, that is, $t_f = (\delta/g)^{1/2}$. Thus,

$$x_r \sim U_1 t_f = U_1(\delta/g)^{1/2} \tag{2}$$

Equation (2) suggests that the dimensionless range of the ballistic path, $X_r = (x_r/\delta)$, must follow a linear relation with a modified Froude number defined as, $Fr_g = Fr_{\Delta h}\sqrt{\Delta h^*} = U_1/\sqrt{g(h_g - h_1)}$, where $\Delta h^* = \frac{\Delta h}{\delta} = \frac{h_0 - h_g}{h_g - h_1}$ is the maximum available water height difference, made dimensionless with the height of the plate's edge, $h_g$, relative to the free surface depth $h_1$. Therefore, $X_r$ should increase proportionally to $Fr_g$.

Figure 9b shows the experimental values of the dimensionless range, $X_r$, as a function of the Froude number, $Fr_g$, for a wide range of variation of $\Delta h$ and $U_1$, shown in Table 2. The range $x_r$ is experimentally measured from the top view images (see Fig. 6a) as the distance between the plate and the location of the splash point. Since the impingement point when $W = 0.3$ and $W = 0.5$ is located very close to the side wall, the determination of that point is difficult in these cases. Therefore, only the cases with $W = 0.7$ are displayed. The error bars in Fig. 9b take into account the small oscillations observed in the splash point. For the cases that correspond to spilling waves, a null value was assigned to the range ($x_r = 0$), since there is not a separated jet. Notice that the data are well fitted by a

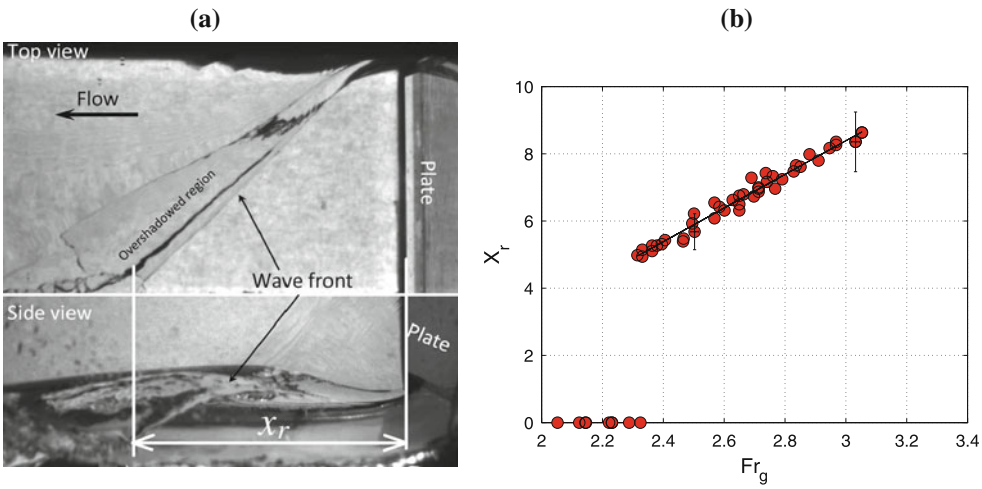


**Fig. 9** **a** *Top* and *side* view of a typical plunging breaker. $x_r$ is defined as the distance between the plate and the impingement point in the downstream direction. **b** Square dimensionless range as a function of the modified Froude number, $Fr_g$ for $W = 0.7$. The linear relation between $X_r$ and $Fr_g$ validates the ballistic trajectory assumption

**Table 2** Ranges of the relevant parameters of the flow used to investigate the ballistic path of the front of the corner wave and the breaking transition

| Type of breaker | $h_g$ (mm) | $h_1$ (mm) | $h_0$ (mm) | $\Delta h$ (mm) | $U_1$ (m/s) | $Fr_{\Delta h}$ | $Fr_g$ |
|---|---|---|---|---|---|---|---|
| Plunging | 95–191 | 32–134 | 175–363 | 77–268 | 1.6–2.1 | 1.40–1.86 | 2.33–3.52 |
| Transition | 95–191 | 67–142 | 175–293 | 74–103 | 1.3–1.7 | 1.65–1.86 | 2.05–2.66 |
| Spilling | 95–191 | 67–142 | 120–265 | 22–98 | 1.3–1.7 | 1.65–2.76 | 2.05–2.66 |

straight line which validates the ballistic trajectory hypothesis of the wave's front given by Eq. (2).

The conclusion that can be drawn from these experiments is that whereas the trajectory of the wave's front is not significantly affected by the distance between the submerged edge of the plate and the channel's bottom, $h_g$, the range of the ballistic flight of the jet, $X_r$, is strongly dependent on this parameter. The explanation is that the formation of the wave is determined by the local structure of the flow near the corner, which is fairly similar to that of a plate immersed into a uniform stream of velocity $U_1$. In the ideal case, the available water height above the corner, $\Delta h$ together with $U_1$ emerge as the only two parameters affecting the flow. In other words, the velocity field near the corner would vary along distances of the order of the flow depth, which are much larger than the size of the wave at the location where the jet detaches. From that point on, changes in the flow field due to the presence of the bottom will not affect the jet trajectory, which is solely determined by the launching conditions.

On the other hand, the range of the ballistic flight of the jet must depend on the height that the jet will fall from its origin. Obviously, the free fall height at the impingement point is determined by the *vena contracta* effect, which leads to the lowering of the free surface far downstream with respect to the height of the corner. It is well known (Montes 1997; Chows 1959) that the water depth far downstream, $h_1$, is proportional to the height of the plate with respect to the bottom, $h_g$; thus, the free fall height, $\delta = (h_g - h_1)$, can be considered to be also proportional to $h_g$.

### 3.4 Plunging spilling transition

In Sect. 3.2, we showed that the slope of the wave's crest and the trajectory of the front are a function of the Froude number based on the depth of penetration of the plate, $Fr_{\Delta h}$. In addition, we observed that, as this parameter increases, the trajectories of the wave separates from the plate, and the wave is predominantly dominated by the liquid's inertia. Conversely, when the Froude number decreases, provided that it must always be greater than the unity in order to maintain the supercritical character of the flow, the trajectories of the wave approach the plate, while enhancing the effect of gravity against the inertia.

At small $Fr_{\Delta h}$ numbers, when the initial potential energy level is large, the crest of the wave is able to separate shortly after being formed and plunges following a ballistic trajectory. However, when $Fr_{\Delta h}$ is increased, the weak potential energy acquired in the wave formation process results in waves whose crest lacks the required energy to separate, that is, spilling waves. Figure 10 shows a summary of the wave characteristics as a function of $Fr_{\Delta h}$. We found that for $Fr_{\Delta h} \leq 1.65$, the waves always plunge. In the range $1.65 \leq Fr_{\Delta h} \leq 1.88$, we found a regime of weak plunging in which the wave's crest no longer separates

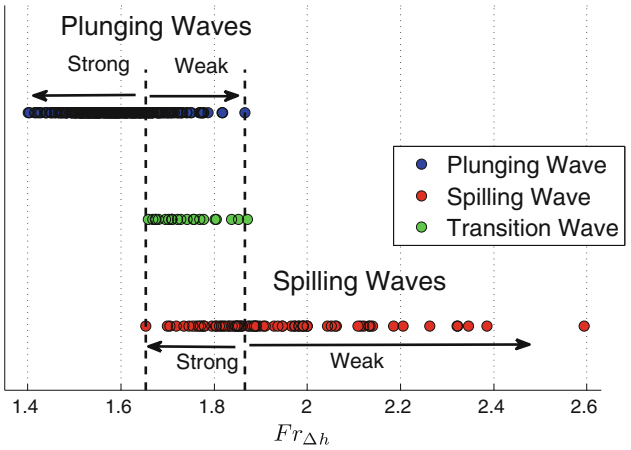


**Fig. 10** Transition diagram between plunging and spilling breakers based on the Froude number $Fr_{\Delta h}$. The *blue color* denotes plunging waves cases whereas *the red* one represents spilling ones. The *green color* is used when it cannot be determined if the wave is either plunging or spilling. Those waves are called "transition waves"

from the face of the wave and the spilling regime begins. As the Froude number is increased above this threshold $Fr_{\Delta h} \simeq 1.88$, only spilling waves are encountered.

## 4 Conclusion

We have analyzed the wave originating at the corner of a partially submerged vertical flat plate, namely the corner wave, as a prototypical flow configuration of nearly 2-D surface gravity waves. The main characteristic of this wave is that it remains stationary in the laboratory reference frame allowing for a detailed, parametric study of its characteristics.

In all our experiments, we have shown that the formation and initial development of the corner wave are unaffected by the presence of the walls and bottom of the channel. This suggests that the formation of the wave is a local phenomenon, in the sense that it depends only on the structure of the flow field near the corner. Therefore, the main dimensionless parameter affecting the initial stages in the evolution of the corner wave is the Froude number $Fr_{\Delta h}$, based on the available water height upstream of the plate, $\Delta h$ This work is theoretically complemented by Martínez-Legazpi et al. (2012).

The amplitude of the corner wave increases as the wave evolves downstream until it eventually develops into either a spilling or a plunging breaker. Our parametric study shows that the transition from spilling to plunging occurs at a critical band of the Froude number. More specifically, we have shown that a transition region, in which plunging and spilling waves coexist, appears when the Froude number $Fr_{\Delta h}$ exceeds the critical value, $Fr_{\Delta h} \geq 1.65$, while when $Fr_{\Delta h} \geq 1.88$, only spilling waves form. The resulting plunging jet is shown to follow a ballistic trajectory, as is the case of time-evolving, two-dimensional plunging breakers.

**Acknowledgments** This work has been partially supported by the ONR under contract N00014-05-1-0121 and the Spanish Ministry of Science through grant: DPI2011-28356-C03-02.

## References

Aliseda A, Lasheras JC (2006) Effect of buoyancy on the dynamics of a turbulent boundary layer laden with microbubbles. J Fluid Mech 559:307–334

Banner ML, Peregrine DH (1993) Wave breaking in deep water. Ann Rev Fluid Mech 25:373–397

Bonmarin P, Ramamonjiarisoa A (1985) Deformation to breaking of deep water gravity waves. Exp Fluids 3:11–16

Chows VT (1959) Open-channel hydraulics. Mcgraw-Hill, New York, pp 00701–07769

Cokelet ED (1977) Breaking waves. Nature 267:769–774

Drazen D, Melville WK, Lenain L (2008) Inertial scaling of dissipation in unsteady breaking waves. J Fluid Mech 611:307–332

Duncan JH (1981) An experimental investigation of breaking waves produced by a towed hydrofoil. Proc R Soc Lond Ser A Math Phys Sci 377(1770):331–348

Duncan JH (2001) Spilling breakers. Ann Rev Fluid Mech 33:519–547

Duncan JH, Philomin V, Behres M, Kimmel J (1994) The formation of spilling breaking water waves. Physics of Fluids 6(8):2558–2560

Duncan JH, Qiao H, Philomin V, Wenz A (1999) Gentle spilling breakers: crest profile evolution. J Fluid Mech 379:191–222

Fontaine E, Tulin MP (1998) On the prediction of nonlinear free-surface flows past slender hulls using 2D+T theory: the evolution of an idea. RTO MP-15

Galvin, Jr CJ (1968) Breaker type on three laboratory beaches. J Geophys Res 73:3651–3659

Hager WH, Mazumder SK (1992) Supercritical flow at abrupt expansions. Proc Inst Civ Eng Water Marit Energy 96:153–166

Hager WH, Yasuda Y (1997) Unconfined expansion of supercritical water flow. J Eng Mech 123:451–457

Iafrati A, Broglia R (2010) Comparisons between 2D+T potential flow models and 3D RANS for planing hull hydrodynamics. In: Proceedings 25th international workshop on water waves and floating bodies, pp 65–69

Richter JP (1970) The notebooks of Leonardo da Vinci. Dover Publications Inc., ISBN 0-486-22573-9

Kiger KT, Duncan JH (2011) Air-entrainment mechanisms in plunging jets and breaking waves. Annu Rev Fluid Mech 44:563–596

Kim D-G (2007) Numerical analysis of free flow past a sluice gate. KSCE J Civ Eng 11(2):127–132

Longuet-Higgins M (1995) On the disintegration of the jet in a plunging breaker. J Phys Oceanogr 25:2458–2462

Martínez-Legazpi P (2011) Corner waves downstream from a partially submerged vertical plate. PhD thesis, Universidad Carlos III de Madrid

Martínez-Legazpi P, Rodríguez-Rodríguez J, Korobkin A, Lasheras JC (2012) Formation of corner waves in the wake of a partially submerged bluff body. J Fluid Mech (submitted to)

Mauer BD, Bolster DT, Linden PF (2010) Intrusive gravity currents between two stably stratified fluids. J Fluid Mech 647:53–69

Melville WK (1996) The role of surface-wave breaking in air–sea interaction. Annu Rev Fluid Mech 28:279–321

Melville WK, Rapp JH (1988) The surface velocity field in steep and breaking waves. J Fluid Mech 189:1–22

Molland A (2008) The maritime engineering reference book. Butterworth-Heinemann, Oxford, p 599. ISBN: 978-0-7506-8987-8

Montes JS (1997) Irrotational flow and real fluid effects under planar sluice gates. J Hydraul Eng ASCE 123:219–232

Munk MM (1924) The aerodynamic forces on airship hulls. NACA report 184

Newman JN (1977) Marine hydrodynamics. MIT Press, Cambridge, p 29. ISBN 0-262-14026-8

Oh S, et al (2005) Experimental investigation of breaking criteria of deep water wind waves under strong wind action. Appl Ocean Res 27:235–250

Rapp JH, Melville WK (1990) Laboratory measurements of deep-water breaking waves. Philos Trans R Soc Lond 331:735–800

Rodríguez-Rodríguez J, Marugán-Cruz C, Aliseda A, Lasheras JC (2011) Dynamics of large turbulent structures in a steady breaker. Exp Therm Fluid Sci 35:301–310

Roth A, Hager WH (1999) Underflow of a standard sluice gate. Exp Fluids 27:339–350

Schultz WW, Huh J, Griffin OM (1994) Potential energy in steep and breaking waves. J Fluid Mech 278:201–228

Shakeri M, Maxeiner E, Fu T, Duncan JH (2009) An experimental examination of the 2D+T approximation. J Ship Res 53:59–67

Shakeri M, Tavakolinejad M, Duncan JH (2009) An experimental investigation of divergent bow waves simulated by a 2D+T technique. J Fluid Mech 634:217–243

Sumer BM, Fredsoe J (1997) Hydrodynamics around cylindrical structures. World Scientific, Singapore, p 129. ISBN: 981022898

Tulin MP (1957) Theory of slender surface planing at high speeds. Schiffstechnik 4, Heft 21, pp 125–133

Tulin MP, Wu M (1997) Divergent bow waves. In: Proceedings of the 21st symposium on naval hydrodynamics, pp 661–669

Wagner H (1932) Über Stoβ und Gleitvorgänge ander Oberfläche von Flüssigkeiten. ZAMM 12:193–215